Science of the Total Environment 912 (2024) 169477

Contents lists available at ScienceDirect

Science of the Total Environment

journal homepage: www.elsevier.com/locate/scitotenv

Weaker regional carbon uptake albeit with stronger seasonal amplitude in northern mid-latitudes estimated by higher resolution GEOS-Chem model

Zhiqiang Liu [a,*], Ning Zeng [b,c,**], Yun Liu [d], Jun Wang [e], Pengfei Han [f,g], Qixiang Cai [g]

[a] CMA Key Open Laboratory of Transforming Climate Resources to Economy, Chongqing Institute of Meteorological Sciences, Chongqing 401147, China
[b] Dept. of Atmospheric and Oceanic Science, University of Maryland, College Park, Maryland, USA
[c] Earth System Science Interdisciplinary Center, University of Maryland, College Park, Maryland, USA
[d] Geochemical and Environment Research Group, Texas A&M University, College Station, TX, USA
[e] International Institute for Earth System Science, Nanjing University, Nanjing, China
[f] Carbon Neutrality Research Center, Institute of Atmospheric Physics, Chinese Academy of Sciences, Beijing, China
[g] Laboratory of Numerical Modeling for Atmospheric Sciences & Geophysical Fluid Dynamics, Institute of Atmospheric Physics, Chinese Academy of Sciences, Beijing, China

HIGHLIGHTS

- Coarse resolution GEOS-Chem model tend to weaken the vertical transport, leading to biases in CO_2 inversion.
- The annual carbon sink estimates at 4°×5° in N. America, E. Asia, and Europe is 40.5 % larger than at 0.5°×0.625°.
- The seasonal strength estimates at 4°×5° are smaller than at 0.5°×0.625°, especially during the non-growing seasons.
- Generally, the larger carbon uptake occurred in areas with denser fossil fuel emissions.

GRAPHICAL ABSTRACT

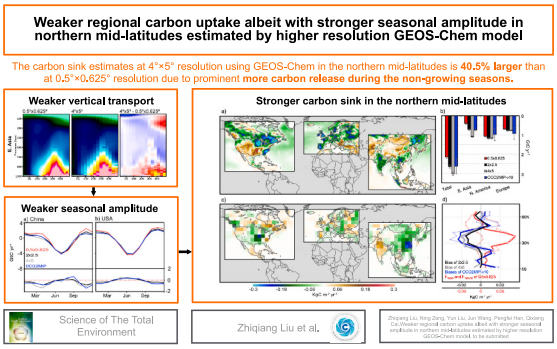

ARTICLE INFO

Editor: Kuishuang Feng

Keywords:
CO_2 inversion
High-resolution transport model
Carbon sink
Seasonal amplitude

ABSTRACT

Terrestrial ecosystem in the Northern Hemisphere is characterized by a substantial carbon sink in recent decades. However, the carbon sink inferred from atmospheric CO_2 data is usually larger than process- and inventory-based estimates, resulting in carbon release or near-neutral carbon exchange in the tropics. The atmospheric approach is known to be uncertain due to systematic biases of coarse atmospheric transport model simulation. Compared to a coarse-resolution inverse estimate at 4° × 5° using GEOS-Chem in the integrated region of N. America, E. Asia, and Europe from 2015 to 2018, the annual carbon sink estimate at a native high-resolution of 0.5° × 0.625° is reduced from −3.0±0.08 gigatons of carbon per year (GtC yr^{-1}) to −2.15±0.08 GtC yr^{-1} due to prominent more carbon release during the non-growing seasons. The major reductions concentrate in the mid-latitudes (20°N–45°N), where the mean land carbon sinks in China and the USA are reduced from 0.64±0.03 and 0.35±0.02 GtC yr^{-1} to 0.14±0.03 and 0.15±0.02 GtC yr^{-1}, respectively. The coarse-resolution GEOS-Chem tends to trap both the release and uptake signal within the planetary boundary layer, resulting in weaker

* Corresponding author.
** Correspondence to: N. Zeng, Dept. of Atmospheric and Oceanic Science, University of Maryland, USA.
E-mail addresses: liuzq961026@gmail.com (Z. Liu), zeng@umd.edu (N. Zeng).

https://doi.org/10.1016/j.scitotenv.2023.169477
Received 13 September 2023; Received in revised form 27 November 2023; Accepted 16 December 2023
Available online 22 December 2023

estimates of biosphere seasonal strength. Since the strong fossil fuel emissions are persistently released from the surface, the trapped signal leads to the stronger estimates of annual carbon uptakes. These results suggest that high-resolution inversion with accurate vertical and meridional transport is urgently needed in targeting national carbon neutrality.

1. Introduction

The carbon sinks of the terrestrial ecosystems and ocean are increasing, generally in pace with the increasing anthropogenic carbon dioxide (CO_2) emissions, which plays an important role in buffering the increasing trend of mean atmospheric CO_2 concentration and the global warming (Friedlingstein et al., 2022). Atmospheric CO_2 records since the 1960s show a significant seasonal cycle that originates mainly from the Northern Hemisphere (NH) terrestrial ecosystems (Keeling, 1960). The large carbon uptake in NH during spring and summer is offset by the large carbon release during autumn and winter, leaving a small annual carbon uptake, on average, in the recent decades (Ciais et al., 1995, 2019; Pan et al., 2011; Schimel et al., 2015). Therefore, a robust annual sink estimate in the NH depends critically on the accuracy of the reproduced seasonal cycle. The carbon sink estimate from the "top-down" approach of atmospheric inversion is usually larger than the "bottom-up" approaches of process-based model simulation and inventory by around 1 gigaton of carbon per year (GtC yr^{-1}) (Schimel et al., 2015) which is about half of the global annual land uptake (Kondo et al., 2020). Based on vertical gradients of airborne CO_2 observations, the strong sink is dramatically reduced by 1.5 GtC yr^{-1} based on the statistic fitting of an ensemble of top-down estimates (Stephens et al., 2007).

The "top-down" approach uses an atmospheric transport model (ATM) driven by meteorological reanalysis products to relate the surface carbon fluxes with observed CO_2 concentration, in which the uncertainty related to the transport simulation is always ignored. Despite many efforts to improve ATM, various transport errors still exist, challenging the reliability of annual carbon budget estimates, especially in the context of the large seasonal cycle amplitude (Baker et al., 2006; Basu et al., 2018; Liu et al., 2011; Schuh et al., 2019, 2022; Stanevich et al., 2020; Yu et al., 2018). One major error originates from the spatiotemporal averaging process of meteorological data that weakens the vertical motion within the boundary layer and amplifies the meridional transport in the northern mid-latitudes (Schuh et al., 2019; Schuh and Jacobson, 2023). Considering such prominent errors, inversions at native high resolution are urgently needed to support reliable national carbon budget accounting (Byrne et al., 2023; Jiang et al., 2022). Since the native high-resolution global inversion is computationally expensive, global inversions were usually conducted at a horizontal resolution of 2° to 5° (Byrne et al., 2023; Friedlingstein et al., 2022) which is about an order of magnitude coarser than state-of-the-art meteorology reanalysis (Gelaro et al., 2017; Hersbach et al., 2020). In this study, we developed a computationally efficient atmospheric inversion framework based on the ATM, GEOS-Chem. It can run at coarse horizontal resolutions of 4° × 5° and 2° × 2.5° over the globe and native high resolution of 0.5° × 0.625° over E. Asia, N. America, and Europe. Based on the inversions at the three horizontal resolutions, we, for the first time, systematically derived the impact of coarse GEOS-Chem on estimating the carbon budget and seasonal cycle in the northern mid-latitudes. Section 2 describes the data and method; Section 3 shows the results; the discussion and conclusion are presented in Sections 4 and 5, respectively.

2. Data and methods

2.1. CO_2 observations

In this study, COLA assimilated surface and satellite observations. The in-situ and flask observations near the surface are obtained from the Obspack_co2_1_GLOBALVIEWplus_v8.0_2022-08-27 dataset (Cox et al., 2022). Sites within the dataset that can represent large-scale CO_2 signals are selected (Fig. S2). We use the land-nadir and land-glint retrieval from the Orbiting Carbon Observatory-2 (OCO-2) based on the Atmospheric Carbon Observations from Space (ACOS) algorithm of version 10 (Fig. S1). The high-frequency retrieval is averaged to 10-second bins (Baker et al., 2021). Because there are rare vertical profiles in E. Asia and Europe, several aircraft vertical CO_2 profiles above N. America within the Obspack are used to evaluate the inversion results and to demonstrate that native resolution inversion is better than the coarse resolution inversions. In addition, the Total Carbon Column Observing Network (TCCON) is also used to evaluate the results (Wunch et al., 2011). The details of processing the observations are described in Text S1.

2.2. Inversion system and experiment setup

We use an ensemble-based CO_2 data assimilation system, Carbon in Ocean-Land-Atmosphere (COLA), to relate the observed CO_2 concentration with the surface carbon fluxes. The ATM used in COLA is the GEOS-Chem of version 13.0.2 which allows one-way nesting in a region of interest (Bey et al., 2001). To speed up the model and save the computational resources, the ensemble CO_2 simulations are conducted using a single GEOS-Chem program. The details of GEOS-Chem configurations are described in Text S2. We conducted two global inversion experiments at 4° × 5° (EXP-low) and 2° × 2.5° (EXP-mid) resolutions using coarse meteorological fields of Modern-Era Retrospective analysis for Research and Applications, version 2 (MERRA-2) from NASA Global Modeling and Assimilation Office (Gelaro et al., 2017). The parent model of MERRA-2 is the Goddard Earth Observing System (GEOS) model using the cubed-sphere grid and the analysis outputs are regrided to the latitude-longitude grid at 0.5° × 0.625° resolution (Molod et al., 2015). Furthermore, we conducted a regional experiment at native 0.5° × 0.625° (EXP-high) resolution in N. America, Europe, and E. Asia. All the three experiments are configured with 47 vertical levels. The experiments span from 1 September 2014 to the end of 2018. The initial CO_2 and flux conditions at 1 September 2014 in the three experiments are identical and are generated from a Greenhouse gases Observing SATellite-based inversion at 2° × 2.5° resolution (Yokota et al., 2009). The 1-hourly boundary CO_2 condition for EXP-high is generated from EXP-mid.

The data assimilation algorithms used in COLA are a local ensemble transform Kalman filter (LETKF) with four-dimensional extension (Hunt et al., 2007; Liu et al., 2019), a constrained ensemble Kalman filter (CEnKF) (Liu et al., 2022), and an Assimilating A Priori as special Observation (AAPO) algorithm (Liu et al., 2023). The LETKF is configured to digest asynchronous hourly CO_2 observations within the observation window of 7 days, and to update the flux parameter and CO_2 state at the end of the assimilation window of 1 day. Besides the common CO_2 observations, COLA can digest the spatial gradient of a "bottom-up" estimation as a special observation for the purpose of regularization, which can reduce the bias impact of bottom-up estimation. The spatial gradient of a "bottom-up" estimation or the "bottom-up" estimation itself is called a priori estimation in COLA. The LETKF algorithms can be summarized in the analysis equations,

$$\overline{\mathbf{x}}^{a} = \overline{\mathbf{x}}^{b} + \mathbf{X}^{b}\widetilde{\mathbf{P}}^{a}\left(\mathbf{Y}^{b}\right)^{T}\mathbf{R}^{-1}\left(\mathbf{y}^{o} - \overline{\mathbf{y}}^{b}\right), \quad (1)$$

$$\widetilde{\mathbf{P}}^{\mathbf{a}} = \left[(\mathbf{Y}^{\mathbf{b}})^{\mathrm{T}} \mathbf{R}^{-1} (\mathbf{Y}^{\mathbf{b}}) + (\mathrm{K}-1)\mathbf{I} \right]^{-1}, \quad (2)$$

$$\mathbf{X}^{\mathbf{a}} = \mathbf{X}^{\mathbf{b}} [(\mathrm{K}-1)\widetilde{\mathbf{P}}^{\mathbf{a}}]^{\frac{1}{2}}, \quad (3)$$

where the flux parameter $\mathbf{f}$ is augmented to the CO_2 state $\mathbf{c}$ that $\mathbf{x} = [\mathbf{c}, \mathbf{f}]^{\mathbf{T}}$; the superscripts a and b denote the analysis and background (first guess), respectively, and the background flux is the persistence of analysis flux at the last assimilation time; $\overline{\mathbf{x}}$ and $\mathbf{X}$ are the ensemble mean and ensemble perturbation, respectively; $\mathbf{y}^{\mathrm{o}}$ is the CO_2 observations within the observation window of 7 days and the spatial gradient of a "bottom-up" estimation at the end of assimilation window; $\overline{\mathbf{y}}^{\mathbf{b}}$ is the forecasted ensemble mean observations corresponding to each observations; $\mathbf{Y}^{\mathrm{b}}$ is the ensemble perturbation in the observation space; $\mathbf{R}$ is the observation error matrix; $\widetilde{\mathbf{P}}^{\mathrm{a}}$ is the analysis error covariance; K is the ensemble size which is set to 20; and $\mathbf{I}$ is the identical matrix. The details of generating the ensemble flux uncertainty are described in Text S3. The CEnKF is dedicated to the global mass conservation of CO_2 after the LETKF process because COLA updates the CO_2 state directly in the LETKF step,

$$\overline{\mathbf{c}}^{\mathrm{a}+} = \overline{\mathbf{c}}^{\mathrm{a}} + \mathbf{E}^{\mathrm{a}} (\mathbf{h}^{'}\mathbf{E}^{\mathrm{a}})^{\mathrm{T}} \left(\mathbf{h}^{'}\mathbf{E}^{\mathrm{a}} (\mathbf{h}^{'}\mathbf{E}^{\mathrm{a}})^{\mathrm{T}} \right)^{-1} \left(\mathbf{h}^{'}\overline{\mathbf{c}}^{\mathrm{b}} - \mathbf{h}^{'}\overline{\mathbf{c}}^{\mathrm{a}} \right) \quad (4)$$

where $\overline{\mathbf{c}}^{\mathrm{a}+}$ is the CEnKF ensemble mean of the CO_2 state. $\overline{\mathbf{c}}^{\mathrm{a}}$ is the LETKF ensemble mean of CO_2 state. $\mathbf{E}^{\mathrm{a}}$ is the ensemble perturbation of CO_2 after the LETKF process. CEnKF defines the "observations" as the truth with r = 0 to meet the mass conservation purpose.

COLA optimizes two types of fluxes at 1-day timestep, including the ocean-atmosphere carbon flux and the land-atmosphere flux (including fire). Fossil fuel emissions is prescribed and not optimized. The prescribed emissions are based on a combination of the 1 km × 1 km and the 1° × 1° Open source Data Inventory of Anthropogenic CO_2 emission (ODIAC) product (Oda et al., 2018). Because the 1 km × 1 km ODIAC product contains only the fossil fuel combustion, cement production, and gas flaring, while the aviation, marine bunker, and antarctic fishery are available only from the 1° × 1° ODIAC product. The combined emissions are then disaggregated into one hourly timestep based on the Temporal Improvements for Modeling Emissions by Scaling (TIMES) method (Nassar et al., 2013). The a priori land-atmosphere fluxes are modeled by a dynamic vegetation model, VEgetation-Global-Atmosphere-Soil (VEGAS), at 0.5° × 0.5° resolution and one hourly timestep (Zeng et al., 2014). The a priori ocean-atmosphere fluxes are obtained from a daily p_2^{CO} dataset (Rödenbeck et al., 2013). The three types of fluxes are regrided to the horizontal resolution and domain of the corresponding experiments.

2.3. OCO-2 model intercomparison project v10 (OCO2MIP-v10)

The OCO2MIP-v10 collected state-of-the-art CO_2 inversion results from 15 inversion systems, including AMES, Baker, CAMS, CMS-Flux, COLA, CSU, CT, GCASv2, JHU, LoFI, NIES, OU, TM5-4DVar, UT, and WOMBAT (Byrne et al., 2023). The details of OCO2MIP-v10 participants are described in Table S1. We exclude LoFI and COLA for comparison. Because LoFI is not a standard inversion system and COLA is the system we used to infer the high-resolution flux in this study. Each of the OCO2MIP systems conducts 5 experiments under the same protocol. We use the experiment that assimilate the OCO-2 Land-Nadir and Land-Glint and the surface In-Situ (LNLGIS) observations to compare with our inversion results.

3. Results

3.1. Annual mean

Over 2015–2018, we report the annual mean carbon sinks for the integrated three regions of −2.15±0.08, −2.65±0.09, and −3.02±0.08 gigatons of carbon per year (GtC yr^{-1}) for EXP-high, EXP-mid, and EXP-low, respectively (Fig. 1b). EXP-mid and EXP-low give 23.2 % and 40.5 % more sink estimates than EXP-high, respectively. The stronger carbon uptake estimates from EXP-mid and EXP-low are also shown in each of the three regions, especially E. Asia. The estimates from EXP-mid are well consistent with the ensemble mean estimates of version 10 of the OCO-2 flux model intercomparison project that assimilated the similar observations. Spatially, these stronger carbon uptakes occur mainly in Eastern mainland China and Southern USA (Fig. 1c), resulting in more than 4 times and 1 times larger carbon sink estimation for EXP-low than EXP-high in China and the USA, respectively (Fig. 2). The China's carbon sink estimate of 0.14±0.03 GtC yr^{-1} for EXP-high is smaller than previous inversion studies (He et al., 2023; Jiang et al., 2016; Jin et al., 2023; Kou et al., 2023; Schuh et al., 2022; Wang et al., 2020; Wang et al., 2022; Zhang et al., 2014; Zhong et al., 2023) but is reconciled with inventory or process-based modeling estimates (Fang et al., 2018; Lu et al., 2018; Piao et al., 2009), albeit in different periods.

The latitudinal distribution of annual mean flux shows a significant overestimation of carbon sink in EXP-mid, EXP-low, and ensemble mean of OCO2MIP-v10 over the mid-latitude of 25°N–45°N, where the fossil fuel emissions are dense (Fig. 1d). Further analysis on how the fossil fuel emissions affect the inverse estimates are shown in Section 3.3. Focusing on the interannual variability, the country-level estimates across the three resolutions are well consistent with each other (Fig. 2). In China and USA, the annual estimates in EXP-high is smaller than EXP-mid and EXP-low for each year, further indicating that the overestimated carbon sink is robust.

3.2. Seasonal cycle

The overestimated annual carbon sink in EXP-mid and EXP-low can be attributed to biases in the seasonal cycle. Recent aircraft campaigns of Atmospheric Carbon and Transport-America find notable underestimation of seasonal strength of N. American biosphere in the OCO2MIP inversions (Cui et al., 2022). Our high-resolution results support this finding and extend it to most NH land areas (Figs. S6 and S7). The main underestimation concentrated in the cropland area of N. America, Central Europe, and China and the Northern forest with strong seasonal cycle.

Generally, both the carbon uptake during the growing seasons and the carbon release during the non-growing seasons are underestimated but differ in magnitude and seasons in different areas (Fig. 3). In China and the USA, EXP-high shows more than 1 times more carbon release and slightly more carbon uptake than EXP-low during the source period and the sink period, respectively (Fig. 3c, d). The systematic seasonal and annual differences among the three experiments display strong seasonality and latitudinal dependency, implying that horizontal coarsening of meteorological data can introduce bias to the flux inversion.

3.3. Transport impact on flux estimates

Coarse-resolution ATM tends to weaken the vertical transport due to the loss of sub-grid-scale eddy mass flux and strengthen the meridional advection due to the increased horizontal diffusion in the mid-latitude of NH in ATM of GEOS-Chem (Schuh et al., 2019; Stanevich et al., 2020; Yu et al., 2018). The direct impact is that a strong flux signal of both uptake and release would be trapped in the planetary boundary layer (PBL) and move northward or southward more quickly in the mid-latitude of NH (Schuh et al., 2019). Below the stratosphere, The vertical distributions of the analysis CO_2 in mid-latitude N. America and E. Asia display annual positive and negative annual biases within the PBL and above the PBL, respectively, in EXP-low (Fig. 4). The strong emissions in the mid-latitudes N. America are ventilated to the high-latitudes, leading to the weak negative annual biases within the PBL in the high-latitudes and the slightly weaker carbon sink in Canada (Fig. 2). In the stratosphere,

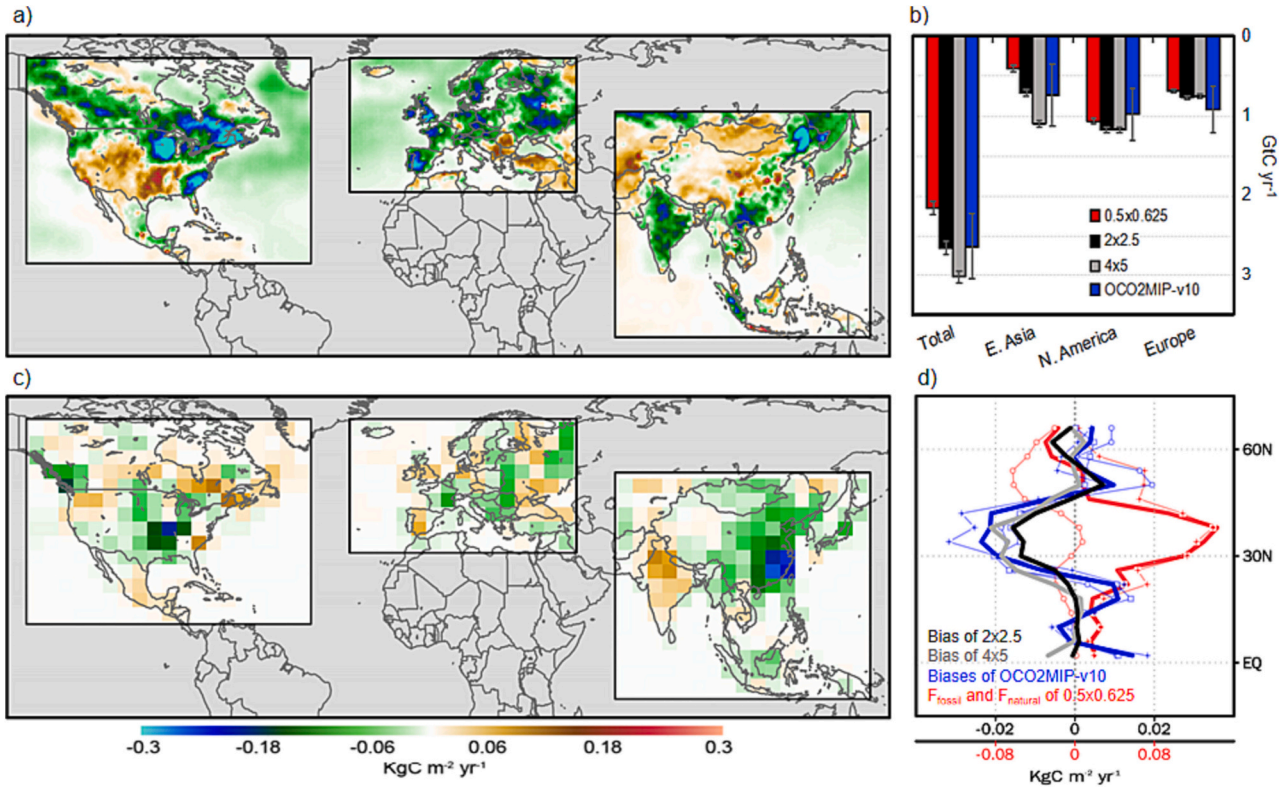

Fig. 1. Terrestrial and ocean carbon fluxes in N. America, E. Asia, and Europe for 2015–2018. a) Annual mean spatial pattern of analysis of carbon fluxes (KgC m^{-2} yr^{-1}) from EXP-high at 0.5° × 0.625° resolution. b) The regional total carbon fluxes (GtC yr^{-1}) from EXP-mid at 2° × 2.5° (black), EXP-low at 4° × 5° (gray), and EXP-high at 0.5° × 0.625° (red) and from ensemble estimates of OCO2MIP-v10 models (blue). The light gray error bars indicate the standard deviation of ensembles. Fig. S3 shows the total estimates in each year. c) Annual mean difference between EXP-low and EXP-high (KgC m^{-2} yr^{-1}). Fig. S5 shows the difference between EXP-mid and EXP-high. d) Latitudinal mean difference per 4° latitude of EXP-mid (black), EXP-low (gray), and the OCO2MIP-v10 ensemble mean (blue) compared to EXP-high. The light blue lines with crosses, circles, and squares marked on are the OCO2MIP-v10 sub-ensemble mean using GEOS-Chem, TM5, and other transport models, respectively. The thick red line is the latitudinal distribution of net fluxes (fossil fuel emissions and natural fluxes of terrestrial and ocean). The light red lines with crosses and circles marked on denote the fossil fuel emissions and the analysis of terrestrial and ocean fluxes in EXP-high, respectively.

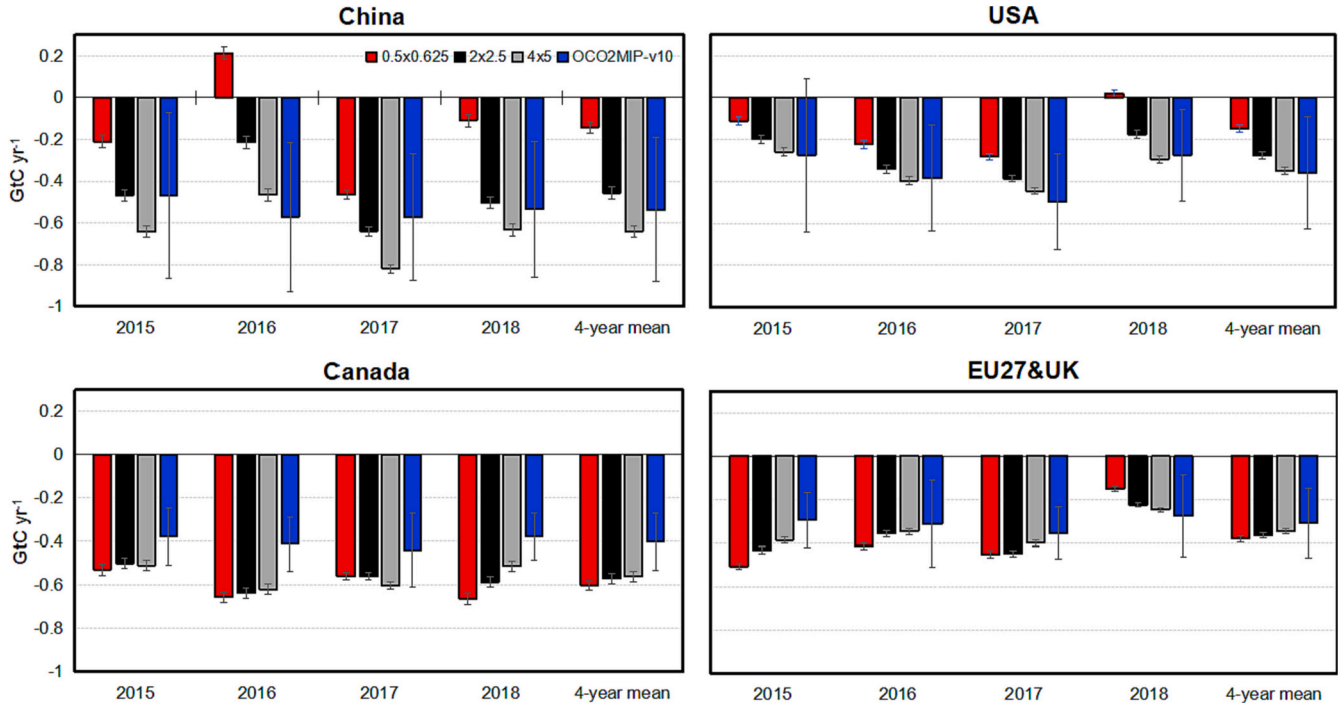

Fig. 2. National terrestrial carbon fluxes (GtC yr^{-1}) for 2015–2018. Note that the regional inversion in N. America does not fully cover the land area of USA and Canada.

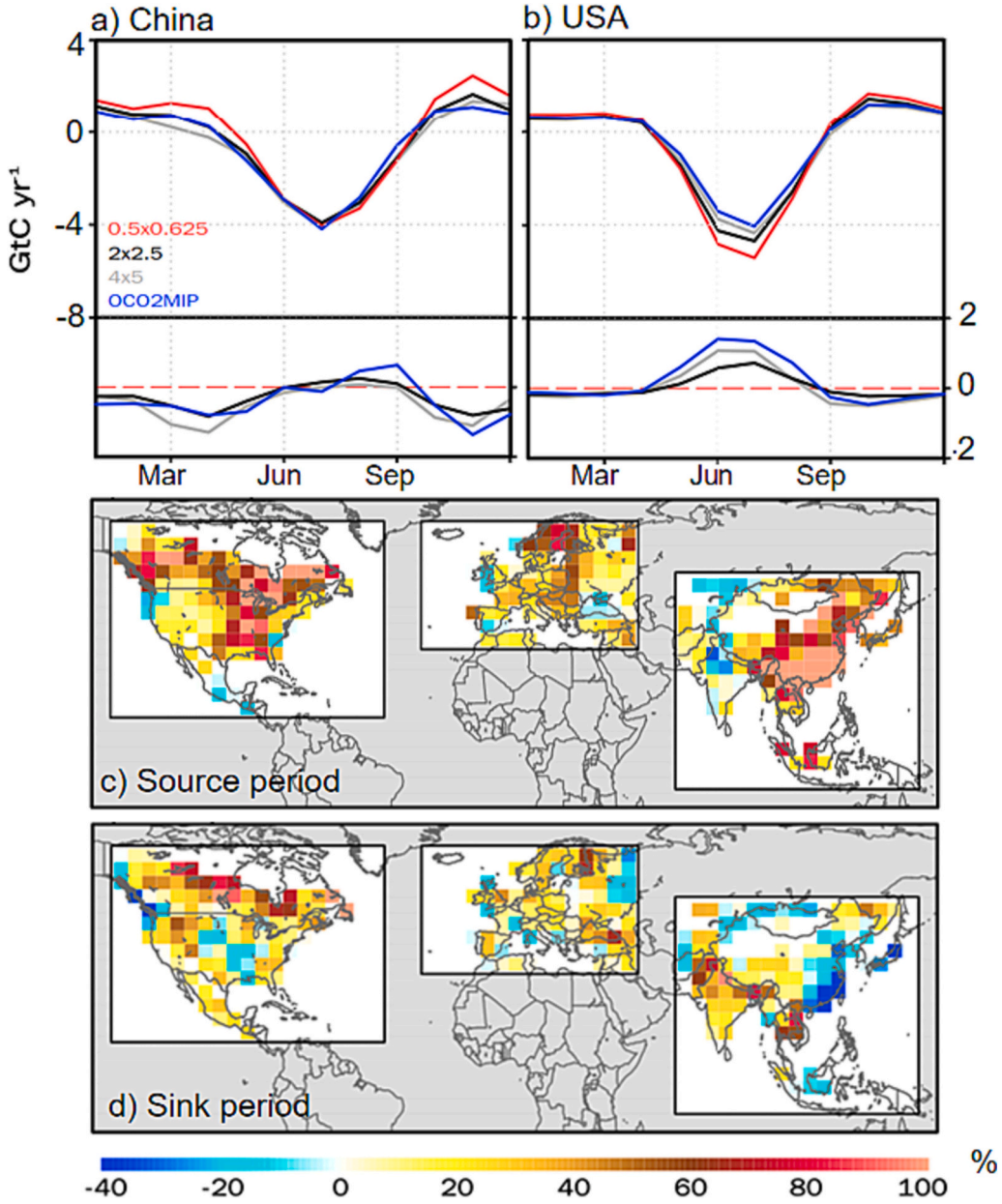

Fig. 3. The stronger seasonal strength of the terrestrial carbon flux in EXP-high than in EXP-low and EXP-mid. The upper subplots in a) and b) show the climatology seasonal cycle in EXP-high (red), EXP-mid (black), EXP-low (gray), and the ensemble mean of OCO2MIP-v10 (blue) in China and the USA, respectively. The bottom subplots in a) and b) show the differences compared to EXP-high. The maps show the ratio calculated by dividing the absolute difference of analysis fluxes between EXP-high and EXP-low by the absolute flux of EXP-low in the c) source and d) sink periods. Fig. S8 shows the comparison between EXP-high and EXP-mid. The source period is the non-growing season when the terrestrial carbon flux is positive, and the sink period is the growing season when the terrestrial carbon flux is negative.

EXP-low displays strong positive annual biases at the mid- and high-latitudes. Stanevich et al. (2020) pointed out that the polar votex barrier at 4° × 5° resolution is weaker than at 2° × 2.5° in GEOS-Chem, resulting in more CO_2 mixed into the stratosphere.

From the inversion perspective, a smaller flux signal in EXP-mid and EXP-low can generate an equivalent near-surface CO_2 signal than in EXP-high, resulting in the stronger annual carbon uptakes and the weaker seasonal cycle amplitude. Moreover, the smaller flux signal trapped in the PBL leads to positive or negative concentration bias when the net flux is released or uptake from the surface, respectively (Fig. 5). This implies that the direction of flux bias depends mainly on the direction of absolute net flux. For the fossil fuel emissions, which is always positive, the bias of PBL CO_2 and the bias of flux are expected to be positive during the entire year. In contrast, the terrestrial could cause opposite biases in growing seasons and decaying seasons. Consequently, in the mid-latitude of E. Asia, the PBL CO_2 biases are positive in each month (Figs. S14 and S15) because of the year-round positive net flux of fossil fuel emissions and terrestrial flux, and the resulting flux bias is negative in most of the months (Fig. 5b). In the mid-latitude of N. America, things are slightly different during the growing seasons that the terrestrial uptake signal overwrites the release signal of fossil fuel emissions, resulting in slight positive flux biases (Fig. 5a). In conclusion, the resulting negative annual flux biases are more a function of the magnitude of underlying fossil fuel emissions.

3.4. Evaluation

The three experiments assimilated the same surface observations in

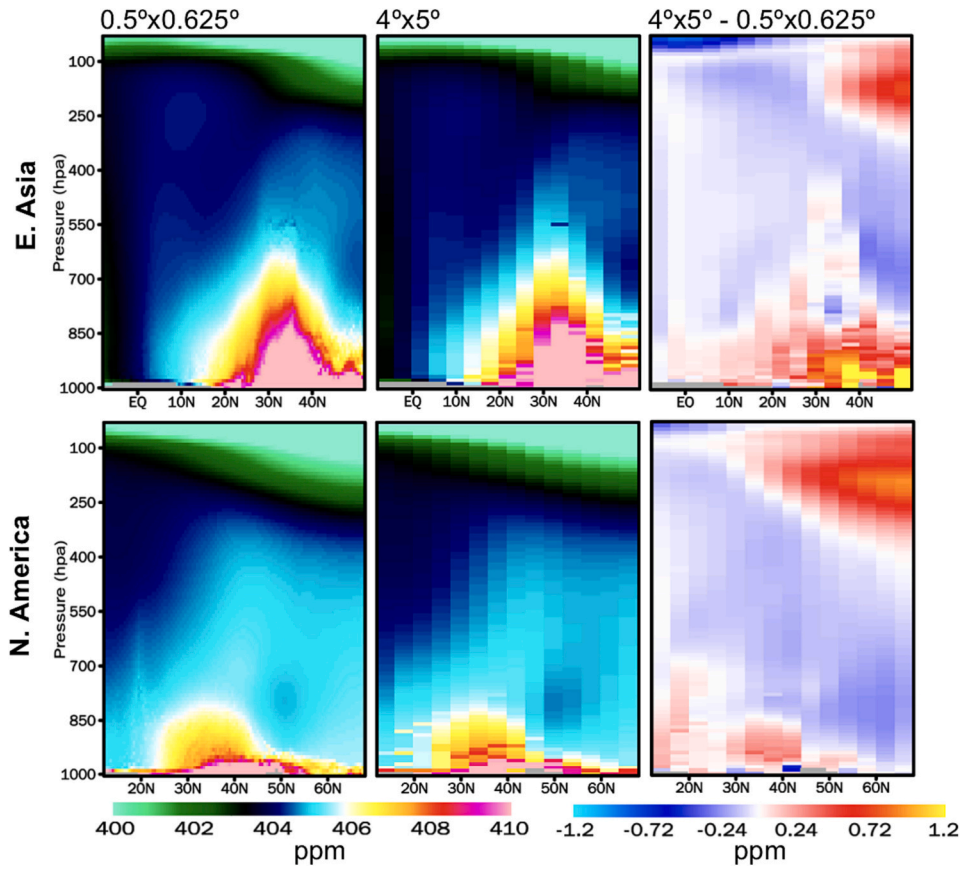

Fig. 4. The 4-year mean vertical-latitude distribution of the analysis CO_2 averaged along the longitude band of (first row) 65°E–135°E in E. Asia and (second row) −105°W–65°W in N. America. The first two columns are the distribution in EXP-high and EXP-low, respectively. The last column is their difference. Figs. S10–12 and S13–15 show the full comparison between the three experiments in E. Asia and N. America, respectively.

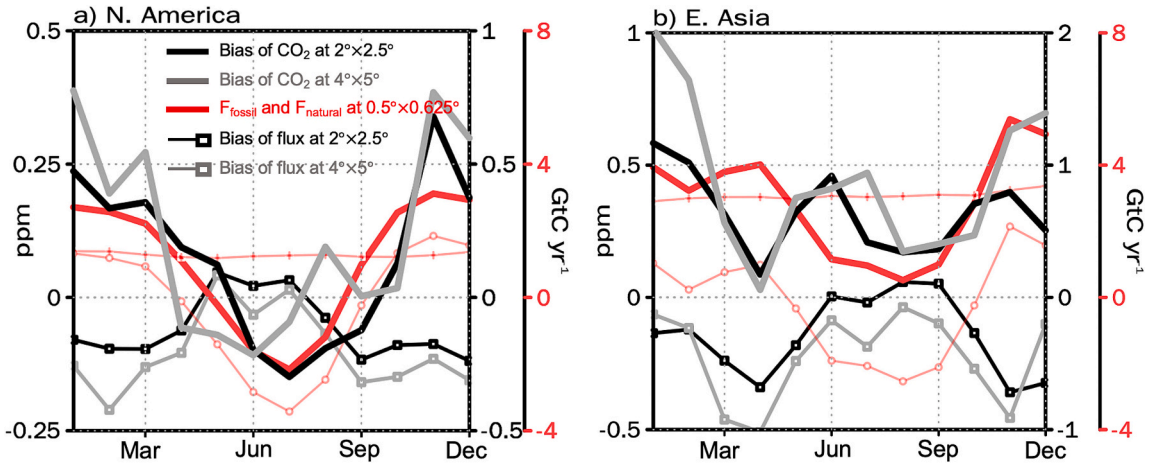

Fig. 5. The climatology seasonal bias of flux and PBL CO_2. Two mid-latitude regions of a) 20°N–45°N, −105°W to −65°W within N. America and b) 20°N–40°N, 65°E to −135°E within E. Asia are considered. The thick gray and black lines are the biases of the analysis of the mean CO_2 concentration under the 850 hpa pressure level for EXP-low and EXP-mid, respectively, compared to EXP-high. The thin gray and black lines with squares marked on are the biases of the analysis of total terrestrial and ocean fluxes within the defined regions for EXP-low and EXP-mid, respectively, compared to EXP-high. The thick red line is the total fluxes of fossil fuel emissions and natural fluxes of terrestrial and ocean for EXP-high. The light red lines with crosses and circles marked on are the fossil fuel emissions and natural fluxes of terrestrial and ocean, respectively, for EXP-high.

the three domains. However, comparing the posterior CO_2 concentration to the assimilated surface observations, the residual absolute biases in EXP-low is significantly greater than EXP-high at most stations, especially over Europe and costal area (Fig. 6a). The coarse resolution ATM can not reproduce the small scale CO_2 variability and clearly separate the boundary between land and ocean, resulting in the greater biases. For the independent TCCON observations (Fig. 6b), the absolute biases in EXP-low is also greater than EXP-high at most stations, suggesting that the posterior CO_2 distribution is improved in EXP-high.

Compared with independent vertical CO_2 profile data in N. America

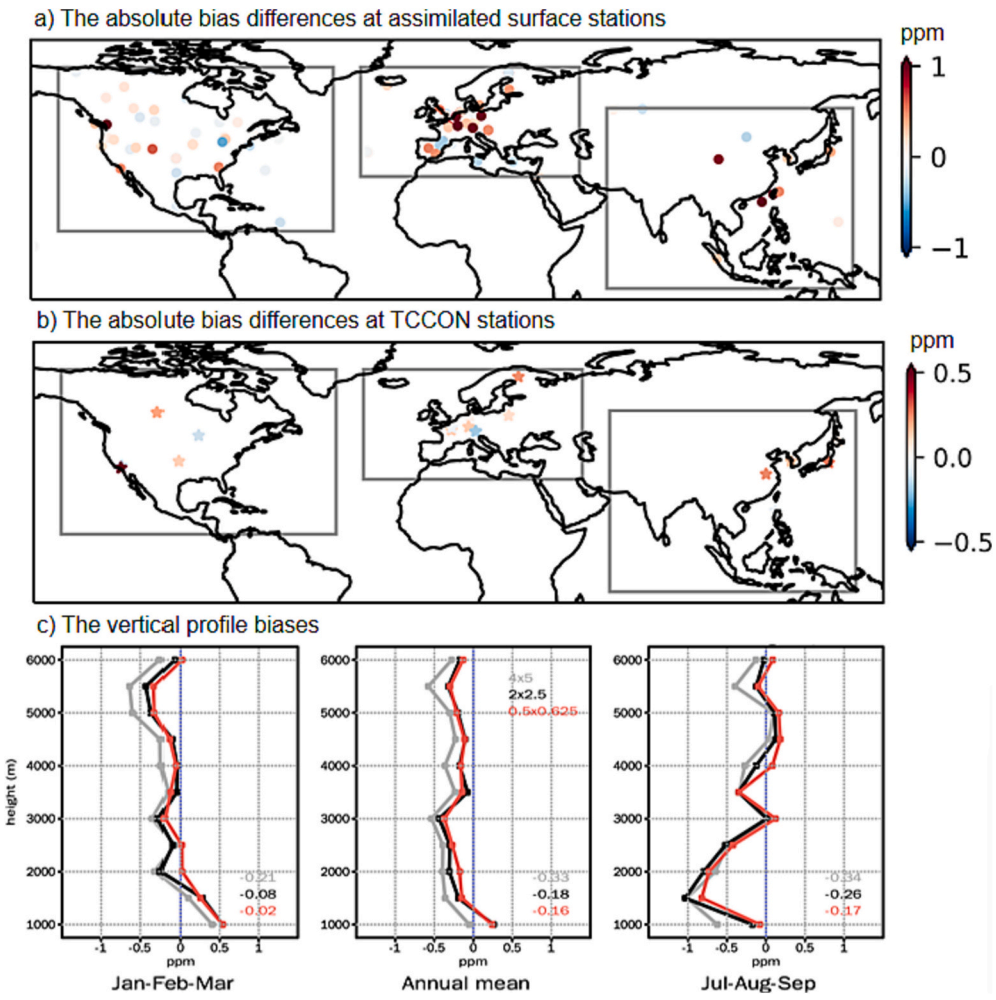

Fig. 6. The absolute annual mean CO_2 and XCO_2 bias differences from 2015 to 2018 between EXP-low and EXP-high for a) assimilated surface observations and b) TCCON observations, respectively. c) The mean vertical CO_2 biases in EXP-high, EXP-mid, and EXP-low compared to 6 vertical CO_2 profiles from 2015 to 2018 (car, hil, cma, crv, esp, and etl) above N. America.

(Fig. 6c), the bias of EXP-high is smaller than EXP-mid and EXP-low, indicating that the inversion at native high resolution improved the estimates and vertical transport. However, in EXP-high, systematic biases still exist, suggesting that the native resolution inversion needs to be further improved.

4. Discussion

In this study, the coarse resolution transport effect on flux estimates is revealed. However, the transport biases still exist in the native resolution GEOS-Chem due to the temporal averaging of meteorology data (Yu et al., 2018). Beside the coarse resolution effect, other factors, e.g., uncertainty from the fossil fuel emissions (Han et al., 2020), satellite retrieval biases (Miller and Michalak, 2020), and representativeness of observations (Wang et al., 2022) may affect the regional estimates. Previous studies pointed out that the fossil fuel emissions in China may be overestimated (Liu et al., 2015) and the magnitude of emissions can affect the estimates of biosphere fluxes (Oda et al., 2023), especially using ATM with systematic biases. Regardless of the absolute size of the carbon sink in Northern mid-latitudes, the tendency of stronger carbon sink using higher resolution GEOS-Chem is robust as revealed in this study. China and USA are the two largest CO_2 emitters worldwide (Friedlingstein et al., 2022). Their terrestrial carbon sink estimates may be overestimated from the previous top-down researches using coarse-resolution GEOS-Chem, thus alleviating their emissions reduction duty. The fundamental issue of ATM bias for the two countries is amplified by their large and persistent fossil fuel emissions and disturbed by the seasonal varying terrestrial flux. In the era of tracing carbon neutrality, accurate accounting of the national CO_2 budget from both top-down and bottom-up perspectives is urgently needed (Byrne et al., 2023; Jiang et al., 2022). Our findings suggest that top-down inversion research equipped with higher resolution and more accurate ATMs is urgently needed (Chevallier et al., 2023; Martin et al., 2022).

5. Conclusion

We conducted two global CO_2 inversions at horizontal resolutions of $4^\circ \times 5^\circ$ and $2^\circ \times 2.5^\circ$, respectively, and a regional CO_2 inversion at the native resolution of $0.5^\circ \times 0.625^\circ$ in the integrated region of N. America, E. Asia, and Europe. Compared to the inversion at $4^\circ \times 5^\circ$ resolution, the carbon sink estimates from the inversion at native resolution in the integrated region are reduced by 40.5 %. The coarse-resolution GEOS-Chem tends to trap both the release signal of fossil fuel emissions and land biosphere respiration and uptake signal of land biosphere photosynthesis within the PBL, resulting in the underestimated seasonal strength of land biosphere. During the non-growing seasons, the coarse resolution inversions shown prominent less carbon release, leading to the overestimated annual carbon sink estimates. Further analysis suggests that the carbon uptakes were overestimated over countries with dense fossil fuel emissions. For example, the mean land carbon sinks in

China and USA are reduced from 0.64±0.03 and 0.35±0.02 GtC yr^{-1} to 0.14±0.03 and 0.15±0.02 GtC yr^{-1}, respectively.

CRediT authorship contribution statement

Zhiqiang Liu: Conceptualization, Data curation, Formal analysis, Investigation, Methodology, Software, Validation, Visualization, Writing – original draft. **Ning Zeng:** Project administration, Resources, Software, Supervision, Writing – review & editing. **Yun Liu:** Software, Writing – review & editing. **Jun Wang:** Writing – review & editing. **Pengfei Han:** Funding acquisition, Supervision. **Qixiang Cai:** Writing – review & editing.

Declaration of competing interest

The authors declare that they have no known competing financial interests or personal relationships that could have appeared to influence the work reported in this paper.

Data availability

The monthly global and regional fluxes and CO_2 fields can be accessed at https://doi.org/10.5281/zenodo.7821665. The OCO2MIP data can be accessed at https://gml.noaa.gov/ccgg/OCO2_v10mip/download.php.

Acknowledgment

We are grateful to the data providers of the NOAA GLOBALVIEW-CO2 ObsPack data and the OCO-2 data. We are grateful to the model developers of GEOS-Chem. We thank Andrew Schuh from Colorado State University for the critical suggestions and comments. We thank the OCO2MIP community for the discussions. This work was supported by the National Natural Science Foundation of China (No. 41975050), the project of "Monitoring, inversion and inventory joint assessment of carbon emissions in typical industrial parks under dual-carbon background" (2022ZJYF001), and the National Key Research and Development Program of China (grant no. 2017YFB0504000).

References

Baker, D.F., Law, R.M., Gurney, K.R., Rayner, P., Peylin, P., Denning, A.S., Bousquet, P., Bruhwiler, L., Chen, Y.-H., Ciais, P., Fung, I.Y., Heimann, M., John, J., Maki, T., Maksyutov, S., Masarie, K., Prather, M., Pak, B., Taguchi, S., Zhu, Z., 2006. TransCom 3 inversion intercomparison: impact of transport model errors on the interannual variability of regional CO_2 fluxes, 1988–2003. Glob. Biogeochem. Cycles 20 (1). https://doi.org/10.1029/2004GB002439.

Baker, D.F., Bell, E., Davis, K.J., Campbell, J.F., Lin, B., Dobler, J., 2021. A new exponentially-decaying error correlation model for assimilating OCO-2 column-average CO_2 data, using a length scale computed from airborne lidar measurements. Geosci. Model Dev. Discuss. 29 https://doi.org/10.5194/gmd-2020-444.

Basu, S., Baker, D.F., Chevallier, F., Patra, P.K., Liu, J., Miller, J.B., 2018. The impact of transport model differences on CO_2 surface flux estimates from OCO-2 retrievals of column average CO_2. Atmos. Chem. Phys. 18 (10), 7189–7215. https://doi.org/10.5194/acp-18-7189-2018.

Bey, I., Jacob, D.J., Yantosca, R.M., Logan, J.A., Field, B.D., Fiore, A.M., Li, Q., Liu, H.Y., Mickley, L.J., Schultz, M.G., 2001. Global modeling of tropospheric chemistry with assimilated meteorology: model description and evaluation. J. Geophys. Res. Atmos. 106 (D19), 23073–23095. https://doi.org/10.1029/2001JD000807.

Byrne, B., Baker, D.F., Basu, S., Bertolacci, M., Bowman, K.W., Carroll, D., Chatterjee, A., Chevallier, F., Ciais, P., Cressie, N., Crisp, D., Crowell, S., Deng, F., Deng, Z., Deutscher, N.M., Dubey, M.K., Feng, S., García, O.E., Griffith, D.W.T., Zeng, N., 2023. National CO_2 budgets (2015–2020) inferred from atmospheric CO_2 observations in support of the global stocktake. Earth Syst. Sci. Data 15 (2), 963–1004. https://doi.org/10.5194/essd-15-963-2023.

Chevallier, F., Lloret, Z., Cozic, A., Takache, S., Remaud, M., 2023. Toward high-resolution global atmospheric inverse modeling using graphics accelerators. Geophys. Res. Lett. 50 (5), e2022GL102135 https://doi.org/10.1029/2022GL102135.

Ciais, P., Tans, P.P., Trolier, M., White, J.W.C., Francey, R.J., 1995. A large northern hemisphere terrestrial CO_2 sink indicated by the $^{13}C/^{12}C$ ratio of atmospheric CO_2. Science 269 (5227), 1098–1102. https://doi.org/10.1126/science.269.5227.1098.

Ciais, P., Tan, J., Wang, X., Roedenbeck, C., Chevallier, F., Piao, S.-L., Moriarty, R., Broquet, G., Le Quéré, C., Canadell, J.G., Peng, S., Poulter, B., Liu, Z., Tans, P., 2019. Five decades of northern land carbon uptake revealed by the interhemispheric CO_2 gradient. Nature 568 (7751), 221–225. https://doi.org/10.1038/s41586-019-1078-6.

Cox, A., Di Sarra, A.G., Vermeulen, A., Manning, A., Beyersdorf, A., Zahn, A., Manning, A., Watson, A., Karion, A., Hoheisel, A., Leskinen, A., Hensen, A., Andrews, Arlyn, Jordan, A., Frumau, A., Colomb, A., Scheeren, B., Law, B., Baier, B., Loh, Z., 2022. Multi-laboratory Compilation of Atmospheric Carbon Dioxide Data for the Period 1957–2021; obspack_co2_1_GLOBALVIEWplus_v8.0_2022-08-27. NOAA Global Monitoring Laboratory. https://doi.org/10.25925/20220808.

Cui, Y.Y., Zhang, L., Jacobson, A.R., Johnson, M.S., Philip, S., Baker, D., Chevallier, F., Schuh, A.E., Liu, J., Crowell, S., Peiro, H.E., Deng, F., Basu, S., Davis, K.J., 2022. Evaluating global atmospheric inversions of terrestrial net ecosystem exchange CO_2 over North America on seasonal and sub-continental scales. Geophys. Res. Lett. 49 (18) https://doi.org/10.1029/2022GL100147.

Fang, J., Yu, G., Liu, L., Hu, S., Chapin, F.S., 2018. Climate change, human impacts, and carbon sequestration in China. Proc. Natl. Acad. Sci. 115 (16), 4015–4020. https://doi.org/10.1073/pnas.1700304115.

Friedlingstein, P., Jones, M.W., O'Sullivan, M., Andrew, R.M., Bakker, D.C.E., Hauck, J., Le Quéré, C., Peters, G.P., Peters, W., Pongratz, J., Sitch, S., Canadell, J.G., Ciais, P., Jackson, R.B., Alin, S.R., Anthoni, P., Bates, N.R., Becker, M., Bellouin, N., Zeng, J., 2022. Global carbon budget 2021. Earth Syst. Sci. Data 14 (4), 1917–2005. https://doi.org/10.5194/essd-14-1917-2022.

Gelaro, R., McCarty, W., Suárez, M.J., Todling, R., Molod, A., Takacs, L., Randles, C.A., Darmenov, A., Bosilovich, M.G., Reichle, R., Wargan, K., Coy, L., Cullather, R., Draper, C., Akella, S., Buchard, V., Conaty, A., da Silva, A.M., Gu, W., Zhao, B., 2017. The modern-era retrospective analysis for research and applications, version 2 (MERRA-2). J. Clim. 30 (14), 5419–5454. https://doi.org/10.1175/JCLI-D-16-0758.1.

Han, P., Zeng, N., Oda, T., Lin, X., Crippa, M., Guan, D., Janssens-Maenhout, G., Ma, X., Liu, Z., Shan, Y., Tao, S., Wang, H., Wang, R., Wu, L., Yun, X., Zhang, Q., Zhao, F., Zheng, B., 2020. Evaluating China's fossil-fuel CO_2 emissions from a comprehensive dataset of nine inventories. Atmos. Chem. Phys. 20 (19), 11371–11385. https://doi.org/10.5194/acp-20-11371-2020.

He, W., Jiang, F., Ju, W., Chevallier, F., Baker, D.F., Wang, J., Wu, M., Johnson, M.S., Philip, S., Wang, H., Bertolacci, M., Liu, Z., Zeng, N., Chen, J.M., 2023. Improved constraints on the recent terrestrial carbon sink over China by assimilating OCO-2 XCO2 retrievals. J. Geophys. Res. Atmos. 128 (14), e2022JD037773 https://doi.org/10.1029/2022JD037773.

Hersbach, H., Bell, B., Berrisford, P., Hirahara, S., Horányi, A., Muñoz-Sabater, J., Nicolas, J., Peubey, C., Radu, R., Schepers, D., Simmons, A., Soci, C., Abdalla, S., Abellan, X., Balsamo, G., Bechtold, P., Biavati, G., Bidlot, J., Bonavita, M., Thépaut, J., 2020. The ERA5 global reanalysis. Q. J. R. Meteorol. Soc. 146 (730), 1999–2049. https://doi.org/10.1002/qj.3803.

Hunt, B.R., Kostelich, E.J., Szunyogh, I., 2007. Efficient data assimilation for spatiotemporal chaos: a local ensemble transform Kalman filter. Phys. D: Nonlinear Phenom. 230 (1–2), 112–126. https://doi.org/10.1016/j.physd.2006.11.008.

Jiang, F., Chen, J.M., Zhou, L., Ju, W., Zhang, H., Machida, T., Ciais, P., Peters, W., Wang, H., Chen, B., Liu, L., Zhang, C., Matsueda, H., Sawa, Y., 2016. A comprehensive estimate of recent carbon sinks in China using both top-down and bottom-up approaches. Sci. Rep. 6 (1), 22130 https://doi.org/10.1038/srep22130.

Jiang, F., He, W., Ju, W., Wang, H., Wu, M., Wang, J., Feng, S., Zhang, L., Chen, J.M., 2022. The status of carbon neutrality of the world's top 5 CO_2 emitters as seen by carbon satellites. Fundam. Res. 2 (3), 357–366. https://doi.org/10.1016/j.fmre.2022.02.001.

Jin, Z., Wang, T., Zhang, H., Wang, Y., Ding, J., Tian, X., 2023. Constraint of satellite CO_2 retrieval on the global carbon cycle from a Chinese atmospheric inversion system. Sci. China Earth Sci. 66 (3), 609–618. https://doi.org/10.1007/s11430-022-1036-7.

Keeling, C.D., 1960. The concentration and isotopic abundances of carbon dioxide in the atmosphere. Tellus 12 (2), 200–203. https://doi.org/10.3402/tellusa.v12i2.9366.

Kondo, M., Patra, P.K., Sitch, S., Friedlingstein, P., Poulter, B., Chevallier, F., Ciais, P., Canadell, J.G., Bastos, A., Lauerwald, R., Calle, L., Ichii, K., Anthoni, P., Arneth, A., Haverd, V., Jain, A.K., Kato, E., Kautz, M., Law, R.M., Ziehn, T., 2020. State of the science in reconciling top-down and bottom-up approaches for terrestrial CO_2 budget. Glob. Chang. Biol. 26 (3), 1068–1084. https://doi.org/10.1111/gcb.14917.

Kou, X., Peng, Z., Zhang, M., Hu, F., Han, X., Li, Z., Lei, L., 2023. The carbon sink in China as seen from GOSAT with a regional inversion system based on the Community Multi-scale Air Quality (CMAQ) and ensemble Kalman smoother (EnKS). Atmos. Chem. Phys. 23 (12), 6719–6741. https://doi.org/10.5194/acp-23-6719-2023.

Liu, J., Fung, I., Kalnay, E., Kang, J.-S., 2011. CO_2 transport uncertainties from the uncertainties in meteorological fields. Geophys. Res. Lett. 38, L12808 https://doi.org/10.1029/2011GL047213.

Liu, Z., Guan, D., Wei, W., Davis, S.J., Ciais, P., Bai, J., Peng, S., Zhang, Q., Hubacek, K., Marland, G., Andres, R.J., Crawford-Brown, D., Lin, J., Zhao, H., Hong, C., Boden, T. A., Feng, K., Peters, G.P., Xi, F., He, K., 2015. Reduced carbon emission estimates from fossil fuel combustion and cement production in China. Nature 524 (7565), 335–338. https://doi.org/10.1038/nature14677.

Liu, Y., Kalnay, E., Zeng, N., Asrar, G., Chen, Z., Jia, B., 2019. Estimating surface carbon fluxes based on a local ensemble transform Kalman filter with a short assimilation window and a long observation window: an observing system simulation experiment test in GEOS-Chem 10.1. Geosci. Model Dev. 12 (7), 2899–2914. https://doi.org/10.5194/gmd-12-2899-2019.

Liu, Z., Zeng, N., Liu, Y., Kalnay, E., Asrar, G., Wu, B., Cai, Q., Liu, D., Han, P., 2022. Improving the joint estimation of CO_2 and surface carbon fluxes using a constrained

ensemble Kalman filter in COLA (v1.0). Geosci. Model Dev. 15, 5511–5528. https://doi.org/10.5194/gmd-15-5511-2022.

Liu, Z., Zeng, N., Liu, Y., Kalnay, E., Asrar, G., Cai, Q., Han, P., 2023. Assimilating the dynamic spatial gradient of a bottom-up carbon flux estimation as a unique observation in COLA (v2.0). Geosci. Model Dev. Discuss. https://doi.org/10.5194/gmd-2023-15 [Preprint].

Lu, F., Hu, H., Sun, W., Zhu, J., Liu, G., Zhou, W., Zhang, Q., Shi, P., Liu, X., Wu, X., Zhang, L., Wei, X., Dai, L., Zhang, K., Sun, Y., Xue, S., Zhang, W., Xiong, D., Deng, L., Yu, G., 2018. Effects of national ecological restoration projects on carbon sequestration in China from 2001 to 2010. Proc. Natl. Acad. Sci. 115 (16), 4039–4044. https://doi.org/10.1073/pnas.1700294115.

Martin, R.V., Eastham, S.D., Bindle, L., Lundgren, E.W., Clune, T.L., Keller, C.A., Downs, W., Zhang, D., Lucchesi, R.A., Sulprizio, M.P., Yantosca, R.M., Li, Y., Estrada, L., Putman, W.M., Auer, B.M., Trayanov, A.L., Pawson, S., Jacob, D.J., 2022. Improved advection, resolution, performance, and community access in the new generation (version 13) of the high-performance GEOS-Chem global atmospheric chemistry model (GCHP). Geosci. Model Dev. 15 (23), 8731–8748. https://doi.org/10.5194/gmd-15-8731-2022.

Miller, S.M., Michalak, A.M., 2020. The impact of improved satellite retrievals on estimates of biospheric carbon balance. Atmos. Chem. Phys. 20 (1), 323–331. https://doi.org/10.5194/acp-20-323-2020.

Molod, A., Takacs, L., Suarez, M., Bacmeister, J., 2015. Development of the GEOS-5 atmospheric general circulation model: evolution from MERRA to MERRA2. Geosci. Model Dev. 8 (5), 1339–1356. https://doi.org/10.5194/gmd-8-1339-2015.

Nassar, R., Napier-Linton, L., Gurney, K.R., Andres, R.J., Oda, T., Vogel, F.R., Deng, F., 2013. Improving the temporal and spatial distribution of CO_2 emissions from global fossil fuel emission data sets. J. Geophys. Res. Atmos. 118 (2), 917–933. https://doi.org/10.1029/2012JD018196.

Oda, T., Maksyutov, S., Andres, R.J., 2018. The Open-source Data Inventory for Anthropogenic CO_2, version 2016 (ODIAC2016): a global monthly fossil fuel CO_2 gridded emissions data product for tracer transport simulations and surface flux inversions. Earth Syst. Sci. Data 10 (1), 87–107. https://doi.org/10.5194/essd-10-87-2018.

Oda, T., Feng, L., Palmer, P.I., Baker, D.F., Ott, L.E., 2023. Assumptions about prior fossil fuel inventories impact our ability to estimate posterior net CO_2 fluxes that are needed for verifying national inventories. Environ. Res. Lett. 18 (12), 124030 https://doi.org/10.1088/1748-9326/ad059b.

Pan, Y., Birdsey, R.A., Fang, J., Houghton, R., Kauppi, P.E., Kurz, W.A., Phillips, O.L., Shvidenko, A., Lewis, S.L., Canadell, J.G., Ciais, P., Jackson, R.B., Pacala, S.W., McGuire, A.D., Piao, S., Rautiainen, A., Sitch, S., Hayes, D., 2011. A large and persistent carbon sink in the world's forests. Science 333 (6045), 988–993. https://doi.org/10.1126/science.1201609.

Piao, S., Fang, J., Ciais, P., Peylin, P., Huang, Y., Sitch, S., Wang, T., 2009. The carbon balance of terrestrial ecosystems in China. Nature 458 (7241), 1009–1013. https://doi.org/10.1038/nature07944.

Rödenbeck, C., Keeling, R.F., Bakker, D.C.E., Metzl, N., Olsen, A., Sabine, C., Heimann, M., 2013. Global surface-ocean p_2^{CO} and sea–air CO_2 flux variability from an observation-driven ocean mixed-layer scheme. Ocean Sci. 9 (2), 193–216. https://doi.org/10.5194/os-9-193-2013.

Schimel, D., Stephens, B.B., Fisher, J.B., 2015. Effect of increasing CO_2 on the terrestrial carbon cycle. Proc. Natl. Acad. Sci. 112 (2), 436–441. https://doi.org/10.1073/pnas.1407302112.

Schuh, A.E., Jacobson, A.R., 2023. Uncertainty in parameterized convection remains a key obstacle for estimating surface fluxes of carbon dioxide. Atmos. Chem. Phys. 23 (11), 6285–6297. https://doi.org/10.5194/acp-23-6285-2023.

Schuh, A.E., Jacobson, A.R., Basu, S., Weir, B., Baker, D., Bowman, K., Chevallier, F., Crowell, S., Davis, K.J., Deng, F., Denning, S., Feng, L., Jones, D., Liu, J., Palmer, P.I., 2019. Quantifying the impact of atmospheric transport uncertainty on CO_2 surface flux estimates. Glob. Biogeochem. Cycles 33 (4), 484–500. https://doi.org/10.1029/2018GB006086.

Schuh, A.E., Byrne, B., Jacobson, A.R., Crowell, S.M.R., Deng, F., Baker, D.F., Johnson, M.S., Philip, S., Weir, B., 2022. On the role of atmospheric model transport uncertainty in estimating the Chinese land carbon sink. Nature 603 (7901), E13–E14. https://doi.org/10.1038/s41586-021-04258-9.

Stanevich, I., Jones, D.B.A., Strong, K., Parker, R.J., Boesch, H., Wunch, D., Notholt, J., Petri, C., Warneke, T., Sussmann, R., Schneider, M., Hase, F., Kivi, R., Deutscher, N. M., Velazco, V.A., Walker, K.A., Deng, F., 2020. Characterizing model errors in chemical transport modeling of methane: impact of model resolution in versions v9-02 of GEOS-Chem and v35j of its adjoint model. Geosci. Model Dev. 13 (9), 3839–3862. https://doi.org/10.5194/gmd-13-3839-2020.

Stephens, B.B., Gurney, K.R., Tans, P.P., Sweeney, C., Peters, W., Bruhwiler, L., Ciais, P., Ramonet, M., Bousquet, P., Nakazawa, T., Aoki, S., Machida, T., Inoue, G., Vinnichenko, N., Lloyd, J., Jordan, A., Heimann, M., Shibistova, O., Langenfelds, R. L., Denning, A.S., 2007. Weak northern and strong tropical land carbon uptake from vertical profiles of atmospheric CO_2. Science 316 (5832), 1732–1735. https://doi.org/10.1126/science.1137004.

Wang, J., Feng, L., Palmer, P.I., Liu, Y., Fang, S., Bösch, H., O'Dell, C.W., Tang, X., Yang, D., Liu, L., Xia, C., 2020. Large Chinese land carbon sink estimated from atmospheric carbon dioxide data. Nature 586 (7831), 720–723. https://doi.org/10.1038/s41586-020-2849-9.

Wang, Y., Wang, X., Wang, K., Chevallier, F., Zhu, D., Lian, J., He, Y., Tian, H., Li, J., Zhu, J., Jeong, S., Canadell, J.G., 2022. The size of the land carbon sink in China. Nature 603 (7901), E7–E9. https://doi.org/10.1038/s41586-021-04255-y.

Wunch, D., Toon, G.C., Blavier, J.-F.L., Washenfelder, R.A., Notholt, J., Connor, B.J., Griffith, D.W.T., Sherlock, V., Wennberg, P.O., 2011. The total carbon column observing network. Philos. Trans. R. Soc. A Math. Phys. Eng. Sci. 369 (1943), 2087–2112. https://doi.org/10.1098/rsta.2010.0240.

Yokota, T., Yoshida, Y., Eguchi, N., Ota, Y., Tanaka, T., Watanabe, H., Maksyutov, S., 2009. Global concentrations of CO_2 and CH_4 retrieved from GOSAT: first preliminary results. SOLA 5, 160–163. https://doi.org/10.2151/sola.2009-041.

Yu, K., Keller, C.A., Jacob, D.J., Molod, A.M., Eastham, S.D., Long, M.S., 2018. Errors and improvements in the use of archived meteorological data for chemical transport modeling: an analysis using GEOS-Chem v11-01 driven by GEOS-5 meteorology. Geosci. Model Dev. 11 (1), 305–319. https://doi.org/10.5194/gmd-11-305-2018.

Zeng, N., Zhao, F., Collatz, G.J., Kalnay, E., Salawitch, R.J., West, T.O., Guanter, L., 2014. Agricultural Green Revolution as a driver of increasing atmospheric CO_2 seasonal amplitude. Nature 515 (7527), 394–397. https://doi.org/10.1038/nature13893.

Zhang, H.F., Chen, B.Z., van der Laan-Luijkx, I.T., Chen, J., Xu, G., Yan, J.W., Zhou, L.X., Fukuyama, Y., Tans, P.P., Peters, W., 2014. Net terrestrial CO_2 exchange over China during 2001–2010 estimated with an ensemble data assimilation system for atmospheric CO_2. J. Geophys. Res. Atmos. 119 (6), 3500–3515. https://doi.org/10.1002/2013JD021297.

Zhong, J., Zhang, X., Guo, L., Wang, D., Miao, C., Zhang, X., 2023. Ongoing CO_2 monitoring verify CO_2 emissions and sinks in China during 2018–2021. Sci. Bull., S2095927323005674 https://doi.org/10.1016/j.scib.2023.08.039.